PROCEEDINGS, 50th Workshop on Geothermal Reservoir Engineering
Stanford University, Stanford, California, February 10-12, 2025
SGP-TR-229

Update of the 2008 Provisional Enhanced Geothermal Systems (EGS) Assessment for the Great Basin, USA

Erick R. Burns[1], Junyuan Zhang[2], Hongbin Zhan[2], and Colin F. Williams[1]

[1]U.S. Geological Survey, Moffett Field, California, USA

[2]Department of Geology and Geophysics, Texas A&M University, College Station, TX 77843-3115

Corresponding author email: eburns@usgs.gov

Keywords: Geothermal energy resource assessment, heat flow, temperature, EGS

ABSTRACT

In response to the Energy Act of 2020, the U.S. Geological Survey (USGS) is updating the Enhanced Geothermal Systems (EGS) resource assessment for the Great Basin, USA. The previous 2008 provisional assessment estimated how much electricity could be generated from EGS resources of the western United States using models of electric-grade heat, models of heat extraction over time, and estimates of how much rock might be stimulated to produce viable amounts of heat. Herein, a similar conceptual strategy is applied, using updated models of heat extraction as a function of fracture spacing and well distance. Previously used reservoir heat delivery models are updated to have a dependence on fracture and well spacing, potentially improving future estimates of EGS resources as ongoing research provides a better understanding about the success of reservoir stimulation as a function of geology and location. For a range of well distances (250-1000 m) and fracture spacings (1-50 m), heat extraction efficiency ranges from 25-62%, demonstrating the importance of accounting for the most likely results of proven viable fracturing technologies. Although fracturing is important, the biggest uncertainty by far in estimating the EGS resource for the Great Basin is estimating which geologic units at what depths can be stimulated sufficiently to produce geothermal energy economically and efficiently. Uncertainties in these factors yield estimates that range over two orders of magnitude with an upper limit of ~174 terawatts-thermal (TWth) produced for 30 years from the upper 7 km of the crust. This upper limit would require significant technological advances to access most of the electric-grade resource across the Great Basin. Assuming that 1% of this estimate will be accessible in the next few decades gives a resource estimate similar to that made in the 2008 provisional assessment. These estimated EGS heat extraction rates far exceed (>100x) the natural geothermal heat production rate, thus geothermal electricity production at these rates might not be sustainable unless heat is also recharged from other sources (e.g., excess solar energy when supply exceeds demand). In addition to assessment maps and cumulative estimates, the new models of fractured reservoirs developed herein can be used to estimate steady power production given a set of fractures and well spacing, and estimates can be made for setback distances to ensure no thermal interference with nearby powerplants.

1. INTRODUCTION

In response to the Energy Act of 2020, the U.S. Geological Survey (USGS) is updating the 2008 provisional assessment of geothermal resources accessible using Enhanced Geothermal Systems (EGS) in the Great Basin (extent shown in Figure 1; Williams and others, 2008). The 2008 assessment considered resources shallower than 6 km depth that exceed 150 °C. USGS estimated a mean electric power resource on private and accessible public land of approximately 520 GWe (gigawatts-electric) EGS for the western United States, which is similar to resource estimates made by other sources (when restricted to the same depths and geographic extent; Tester and others, 2006; Augustine and others, 2023; and Aljubran and Horne, 2024).

1.1 2008 USGS EGS Models

Williams (2010) summarizes the method of assessing EGS resources for a region. Williams and DeAngelo (2011) describe how uncertainty in temperature and thermal properties translates into uncertainty for regional estimates of cumulative EGS resource potential. In simplified terms, past USGS methods estimate the heat in a reservoir as the product of the volumetric specific heat multiplied by the volume of the reservoir and the temperature above a reference temperature (e.g., the minimum temperature from which electric-grade heat can be extracted). The fraction of this heat that is delivered and converted to electricity is the product of this available heat multiplied by a recovery factor. Williams (2010) states that idealized upper limits of a recovery factor from modeling studies can be as high as 0.5 to 0.6, but that production data from naturally fractured reservoirs yield recovery factors as much as an order of magnitude lower, attributing the poorer real-world performance to geologic heterogeneity and non-uniform fluid flow. Williams (2010) summarizes similarities and differences with the Tester and others (2006) method, noting that concepts are similar, but the definition of terms and choices of estimates are somewhat different. Williams (2010) evaluates the role of depth on fracture properties, concluding that "The geothermal recovery factor, Rg, is likely to decline with increasing effective stress, and to the extent that the increase in effective stress with depth corresponds with increasing temperature in the Earth's crust, the exploitation of deep, high-temperature EGS resources may be limited." A functional form of the variation of recovery factor with depth was not presented at that time.

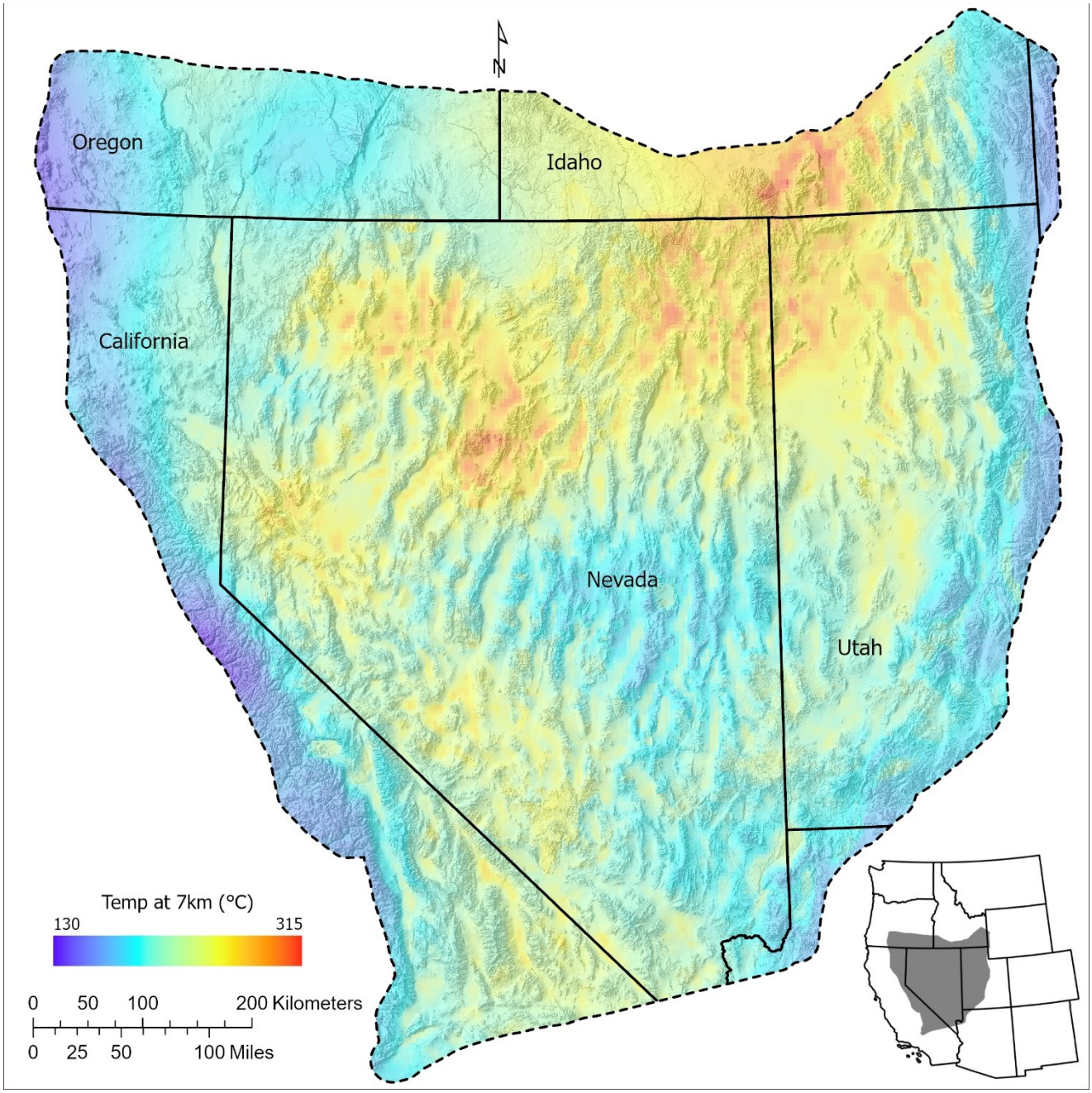

Figure 1: Map of temperature at 7 km depth for the Great Basin, USA (data from Burns and others (2024)). Inset shows the western United States. Hillshade is derived from USGS National Atlas (National Atlas of the United States, 2012).

Because EGS assessment is performed by estimating the available heat (estimated using three-dimensional temperature maps multiplied by density and specific heat capacity of the rock), then estimating the efficiency with which this heat can be extracted as a function of geology (e.g., reservoir models), EGS resource estimation can be improved by using updated three-dimensional temperature maps. As part of the current Great Basin geothermal resource assessment update, Burns and others (2024) estimated the three-dimensional temperature distribution beneath the Great Basin to a depth of 7 km using the methods of Williams and DeAngelo (2011). Improvements in the map include the use of refined estimates of conductive heat flow (DeAngelo and others, 2022, 2023) and calibration of the three-dimensional temperature model using available temperature measurements (Burns and others, 2024a).

1.2 Stimulation Technologies for the Purposes of Geothermal Heat Extraction

An active area of research in EGS reservoir creation is the development of stimulation (e.g., creation of permeability) technologies that reliably produce evenly spaced flowing fractures between two wells at sufficient distance that economic production of heat is sustainable for the design lifetime of a power plant, typically several decades. Flowing fractures in experimental EGS wells are spaced at tens to hundreds of meters (McClure and Horne, 2014), and one goal of stimulation strategies is to optimize spacing. A second goal of stimulation

is to connect an injection and extraction well over long distances. Although the upper limit on distance is poorly understood, researchers tend to use ~1 km or less well spacing for reservoir performance simulations (e.g., Desert Peak simulations of Sanyal and Butler, 2005) which matches induced seismicity/micro-seismicity swarms (presumably accompanied by permeability gains) with lengths of ~1.5 km or less (Figure 16 of Chabora and others, 2012).

2. METHODS

In order to estimate how much heat can be extracted for conversion to electricity in the Great Basin, using analytic solutions, the three-dimensional temperature model of Burns and others (2024a, b) is used to estimate heat that could be delivered from uniformly fractured reservoirs (defined by an effective fracture spacing, which in general is statistically uniform) connected by injection and extraction wells. For these analytic solutions (developed below), it is assumed that reservoir size is sufficiently large such that the fracture spacing can be represented by an effective thermal media (e.g., the reservoir consists of many similarly contributing fractures, instead of only one or two discrete/dominant fractures). That is, at some large reservoir size, heat flow to the repeating pattern of fracture and adjacent conductive block can be replaced with the average heat supplied per unit volume. The representative thermal media is then used to estimate heat delivered from the fractured zone, which is added to heat supplied conductively from the surrounding rock to estimate the total heat delivered for conversion to electricity. Analytic solutions for constant heat extraction rate are used, approximating steady electricity delivery over the power plant design lifetime. The size of the thermally affected region is estimated, allowing an estimate of minimum allowable power plant spacing, and this spacing is used to estimate the total EGS potential for the Great Basin.

2.1 Fractured Reservoir Model

We conceptualize the EGS reservoir as a volume of fractured rock with some effective fracture spacing representing parallel flow paths from an injection well to an extraction well. It is assumed that the temperature of water in the fracture flow paths is uniform across all fractures so that heat leaving the rock can be modeled as one-dimensional cooling at all fractures, and the principle of superposition can be used to estimate the cumulative cooling effect of many fractures. We assume that a power plant will be designed for some power production, and that the ideal situation is an approximately steady rate of heat and electricity production (i.e., the power plant is not over-built, so can be sized for efficiency). Herein, this simplifies to the assumption that heat production rate will be constant over the design life (e.g., 30 years).

Carslaw and Jaeger (1959, p.75) give the following solution for one side of a single fracture with boundary condition of constant prescribed heat flux from the rock:

$$\Delta \mathrm{T}(\mathrm{x},\mathrm{t}) = \frac{2F_0^{single}}{\lambda}\left[\left(\frac{\lambda t}{\pi\rho c}\right)^{1/2} e^{-\frac{\rho c x^2}{4\lambda \mathrm{t}}} - \frac{x}{2} erfc\left(\frac{x}{2\left(\frac{\lambda \mathrm{t}}{\rho c}\right)^{1/2}}\right)\right] \quad (1)$$

Where ΔT is temperature drop from initial uniform temperature (°C), λ is thermal conductivity (W m^{-1} °C^{-1})), ρ is the bulk density of the rock (kg m^{-3}), c is the bulk specific heat capacity of the rock (J kg^{-1} °C^{-1}), x is the distance from the fracture (m), t is time (s), and F_0^{single} is constant heat flux into the fracture (at $x = 0$) from the rock per unit area (W m^{-2}). Unless otherwise stated, for computations herein, a value of 2.7 W m^{-1} °C^{-1} is used as a reasonable overall estimate of reference thermal conductivity for crystalline rock underlying the Great Basin (Burns and others, 2024a). Bulk density and bulk specific heat capacity are assumed to be 2,700 kg m^{-3} and 790 J kg^{-1} °C^{-1}, respectively (Burns and others, 2024a). All estimates herein assume a 30-year operational lifetime where the extraction rate is approximately steady.

The temperature in the fracture (x=0) is given by:

$$\Delta \mathrm{T}_0(\mathrm{t}) = 2F_0^{single}\left(\frac{t}{\pi\lambda\rho c}\right)^{1/2} \quad (2)$$

where the temperature decline is seen to be in the form of a constant multiplied by the square root of time. To estimate the sustainable constant total heat flow from both sides of the fracture (per unit area):

$$2F_0^{single} = \Delta \mathrm{T}_0\left(\frac{\pi\lambda\rho c}{\mathrm{t}}\right)^{1/2} \quad (3)$$

where $\Delta \mathrm{T}_0$ is a difference in temperature from initial uniform conditions (T_0) and temperature at the fracture when reservoir operations will be discontinued ($\mathrm{T}_{exhausted}$) after some prescribed period (t). For example, the reservoir may initially be at 250 °C, and operations will continue at the maximum steady heat flow rate such that the reservoir effluent will reach 100 °C in 30 years. Multiplying $2F_0^{single}$ by the total fracture area gives an estimate of total flow from the reservoir.

Superposition may be applied to equation (2) to estimate the cumulative effect on temperature in each fracture due to pulling some steady heat flux from every fracture ($2F_0$):

$$\Delta \mathrm{T}_0(\mathrm{t}) = 2F_0 \left[\left(\frac{t}{\pi \lambda \rho c} \right)^{1/2} + 2 \sum_{n=1}^{\infty} \left(\left(\frac{t}{\pi \lambda \rho c} \right)^{1/2} e^{-\frac{\rho c n^2 b^2}{4 \lambda \mathrm{t}}} - \frac{nb}{2\lambda} erfc \left(\frac{nb}{\left(\frac{4\lambda \mathrm{t}}{\rho c} \right)^{1/2}} \right) \right) \right] \tag{4}$$

where $2F_0$ is the heat flux in every fracture, b is fracture spacing (m), and n is the number of fractures away from the point of estimation that contribute to the corresponding amount of temperature decline. The summation for an infinite medium in both directions is from $-\infty$ to ∞, but by symmetry, the summation is twice the sum from 1 to ∞, accounting for fractures in both directions. $2F_0$ may be calculated as:

$$2F_0 = \frac{\Delta \mathrm{T}_0(\mathrm{t})}{\left(\frac{t}{\pi \lambda \rho c} \right)^{1/2} + 2 \sum_{n=1}^{\infty} \left(\left(\frac{t}{\pi \lambda \rho c} \right)^{1/2} e^{-\frac{\rho c n^2 b^2}{4 \lambda \mathrm{t}}} - \frac{nb}{2\lambda} erfc \left(\frac{nb}{\left(\frac{4\lambda \mathrm{t}}{\rho c} \right)^{1/2}} \right) \right)} \tag{5}$$

$2F_0$ has been distinguished from $2F_0^{single}$ because the heat fluxes corresponding to the same temperature decline $\Delta \mathrm{T}_0(\mathrm{t})$ will be different, with $F_0 < F_0^{single}$ for each fracture, but the total heat flow for the multi-fracture system is greater (i.e., over time, for the same temperature decline in the fractures, the multiple-fracture system will produce more heat than a single fracture). To get total heat flow from a system of many parallel fractures, $2F_0$ is integrated over the total area of all fractures within the reservoir.

For computational purposes, the infinite sum in equations 4 and 5 can be approximated with a finite number of terms (N) with less than 1% error when the following condition is true:

$$\frac{\frac{1}{1 - e^{-\frac{\rho c b^2}{4\lambda \mathrm{t}}}} - \sum_{n=0}^{N} e^{-\frac{\rho c n b^2}{4\lambda \mathrm{t}}}}{\sum_{n=0}^{N} e^{-\frac{\rho c n^2 b^2}{4\lambda \mathrm{t}}}} \leq 0.01 = 1\% \equiv error\ threshold \tag{6}$$

If a different error is allowable, any value can be used for the $error\ threshold$, but herein, 1% is used. Intuitively, each term in the sum of equations 4 and 5 is the influence of a fracture that is further away, and for any time, some fractures are far enough away that no conductive heat flow signal is felt at any fracture. So, truncation of the infinite sum essentially neglects fractures that are far away.

To estimate the reservoir region as an effective porous media that delivers heat we recognize that, by symmetry, every fracture receives heat from two sides. Symmetry occurs at the halfway point between fractures ($b/2$), so effective heat production per unit volume is:

$$q = \frac{2F_0}{b} \tag{7}$$

where q is in units of (W m^{-3}), and the relation may be applied to any reservoir geometry where the reservoir consists of many fractures.

2.2 Heat Flow from Outside of the Fractured Reservoir

The rock outside the reservoir contributes heat conductively. Although equations (1)-(7) apply to arbitrarily shaped reservoirs, heat flow to the reservoir from outside is generally a function of the surface area to volume ratio, so that the shape controls heat delivery from outside the reservoir. As the distance from the reservoir increases, the reservoir can be approximated as a point with increasing accuracy, and if the subsurface is homogeneous and isotropic, heat flow is radially symmetric towards this point, so solutions with spherical symmetry should apply. Using analytic solutions in terms of dimensionless time and temperature, Elsworth (1990) demonstrated that early behavior of the Fenton Hill test in New Mexico and Rosemanowes Quarry in England circulation tests were well represented by a parallel fracture model, whereas later-time behavior resembled the response of a spherical reservoir model. For models developed and applied herein, the reservoir is conceptualized as connected fractures between two wells, possibly deviating in the path from the straight line. The reservoir is approximated as a spherically shaped region, with the diameter of the sphere estimated as the distance between the injection and extraction wells (with radius in meters; R). Heat delivered from outside the reservoir is a function of reservoir temperature (equation (4)), with more heat delivered when the temperature decline is greater. An upper and a lower bound are developed, allowing an upper and lower estimate of total heat delivered from the reservoir and outside the reservoir.

The upper bound on heat delivered from outside the reservoir is determined by recognizing that superposition still applies, with half of the temperature decline from the repeating fractures inside the reservoir and the other half due to heat extraction from a single side of a fracture (e.g., resembling equation (2), but in spherical coordinates). The reservoir is assumed to be more or less at the uniform temperature given by equation (4), forming the boundary condition for heat conduction from outside. For the upper bound, it is again assumed that heat flux is steady such that we reach the same temperature decline ($\Delta \mathrm{T}_0(\mathrm{t})$) at the end of reservoir life.

For a spherical reservoir of radius R, Carslaw and Jaeger (1959, p. 248) give:

$$\Delta T(r,t) = \frac{R^2 F_0^{radial}}{\lambda r}\left[erfc\left(\frac{r-R}{2\left(\frac{\lambda t}{\rho c}\right)^{1/2}}\right) - e^{\left[\frac{r-R}{R}+\frac{\lambda t}{\rho c R^2}\right]} erfc\left(\frac{r-R}{2\left(\frac{\lambda t}{\rho c}\right)^{1/2}} + \frac{\left(\frac{\lambda t}{\rho c}\right)^{1/2}}{R}\right)\right] \quad (8)$$

where F_0^{radial} is the radial heat flow from outside the reservoir. By superposition, because half of the declines are from within the reservoir, the temperature in the reservoir boundary ($r = R$) is given by equation (8) multiplied by ½ evaluated at $r = R$, plus temperature declines from within the reservoir (equation (4) multiplied by ½):

$$\Delta T_R(t) = \frac{R F_0^{radial}}{2\lambda}\left[1 - e^{\frac{\lambda t}{\rho c R^2}} * erfc\left(\frac{\left(\frac{\lambda t}{\rho c}\right)^{1/2}}{R}\right)\right] + F_0\left[\left(\frac{t}{\pi\lambda\rho c}\right)^{1/2} + 2\sum_{n=1}^{\infty}\left(\left(\frac{t}{\pi\lambda\rho c}\right)^{1/2} e^{-\frac{\rho c n^2 b^2}{4\lambda t}} - \frac{nb}{2\lambda} erfc\left(\frac{nb}{\left(\frac{4\lambda t}{\rho c}\right)^{1/2}}\right)\right)\right] \quad (9)$$

Recall that the value of equation (4) is defined as the design temperature change $\Delta T_0(t)$, and so will equal $\Delta T_R(t)$, allowing simplification of (9) to:

$$\Delta T_R(t) = \Delta T_0(t) = \frac{R F_0^{radial}}{\lambda}\left[1 - e^{\frac{\lambda t}{\rho c R^2}} * erfc\left(\frac{\left(\frac{\lambda t}{\rho c}\right)^{1/2}}{R}\right)\right] \quad (10)$$

which allows estimation of the steady heat flux (per unit area) from outside the reservoir as:

$$F_0^{radial} = \frac{\lambda \Delta T_0(t)}{R\left[1 - e^{\frac{\lambda t}{\rho c R^2}} * erfc\left(\frac{\left(\frac{\lambda t}{\rho c}\right)^{1/2}}{R}\right)\right]} \quad (11)$$

The estimates of equations (9)-(11) overestimate heat flow to the reservoir because the estimated temperature is lower than the reservoir temperature over the design life of the reservoir (Figure 2), and the magnitude of overestimation is a function of fracture spacing within the reservoir. When fracture spacing is larger (Figure 2A), equations (9)-(11) are better estimates than when fracture spacing is smaller, and the temperature decline approaches linear (Figure 2C). Figure 2 uses a constant value for thermal conductivity of 2.7 W m^{-1} $°C^{-1}$ but, in general, thermal conductivity varies as a function of temperature (Williams and DeAngelo, 2011), and the effect of this dependence is considered below for estimating EGS resource potential.

Recognizing that the fractured reservoir temperature (i.e., the boundary condition) is always between equation (9) and the linear decline shown in Figure 2 (the green and dashed lines), an estimate of the lower bound on heat flow from outside the reservoir can be made by assuming the temperature decline in the reservoir is linear. Appendix A shows a derivation for radial convergence of heat from outside a sphere of linearly declining temperature. Converting the notation from Appendix A equation (A.23) to the same notation as equations (9)-(11), the temperature outside the reservoir is:

$$\Delta T(r,t) = \frac{R\Delta T_0^{design}}{r\Delta t_0^{design}}\left\{\left[t * \mathrm{erfc}\left(\frac{r-R}{\left(4\frac{\lambda t}{\rho c}\right)^{1/2}}\right)\right] - \frac{(r-R)^2}{4\frac{\lambda}{\rho c}\pi^{1/2}}\Gamma\left(-1/2, \left[\frac{(r-R)^2}{4\frac{\lambda}{\rho c}t}\right]\right)\right\} \quad (12)$$

where the slope of linear temperature decline is given by design temperature decline (ΔT_0^{design}) over the design lifetime (Δt_0^{design}) in °C and seconds, respectively, and $\Gamma(\omega)$ is the upper incomplete gamma function (integral form shown in Appendix A).

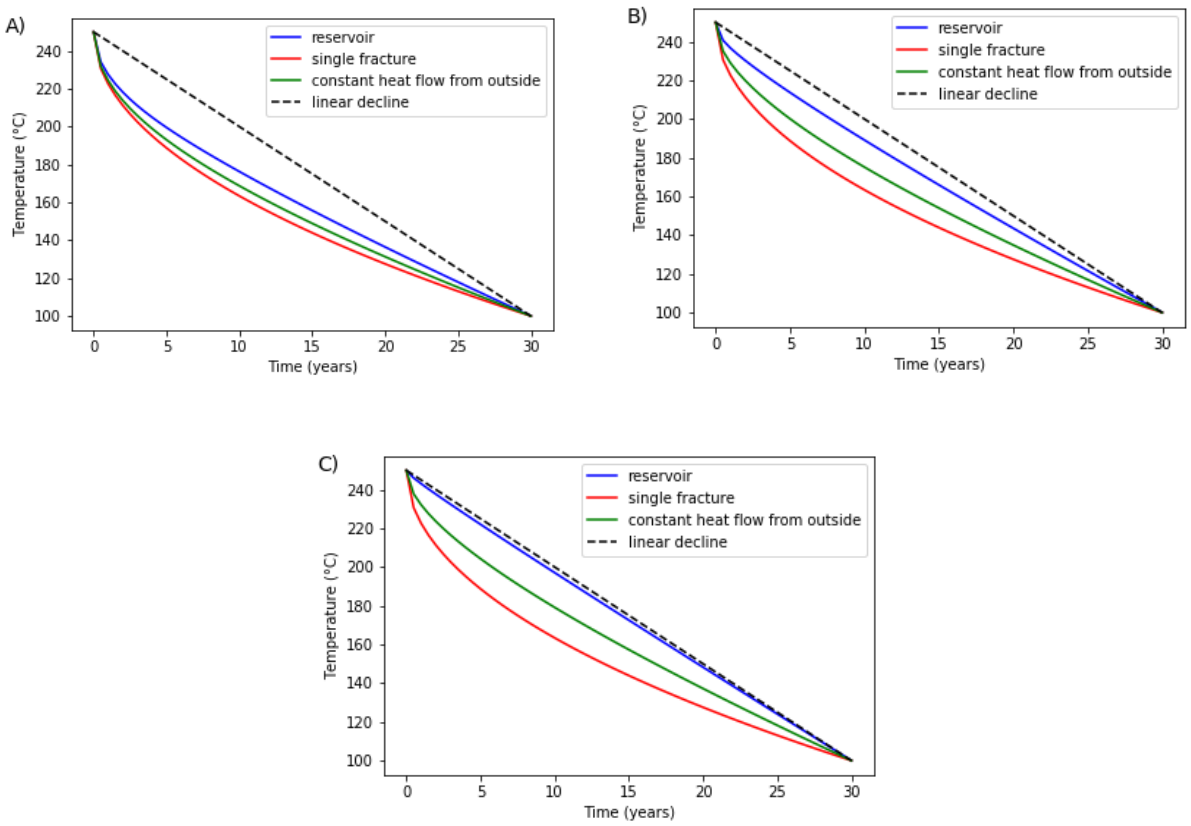

Figure 2: The effect of fracture spacing on reservoir extraction temperature decline (blue lines) for a constant heat extraction rate with starting temperature of 250 ºC and ending temperature of 100 ºC. A) 50-m spacing; B) 20-m spacing; and C) 5-m spacing. As fractures get closer together, reservoir temperature decline approaches a straight line. As fracture spacing gets larger, temperature decline approaches single fracture behavior. The green line shows the decline at the reservoir boundary predicted by equation 9.

The upper incomplete gamma function integral regularly occurs in mathematical physics, so several programming languages have a corresponding function defined, removing the necessity to evaluate the integral numerically. Converting the notation of Appendix A, the heat flux (equation (A.27)) through the spherical boundary corresponding to the linear temperature decline is:

$$F_0^{radial\_linT}(t) = \lambda \frac{\Delta T_0^{design}}{\Delta t_0^{design}} \left[\frac{t}{R} + \left(\frac{4\rho c t}{\lambda \pi} \right)^{1/2} \right] \tag{13}$$

Where the superscript *radial_linT* is used to differentiate this estimate from the estimate generated using equation (11), and the radial heat flux is explicitly noted as a function of time (unlike the constant heat flux of equation (11)). The average heat flow ($\tilde{F}_0^{radial\_linT}$) over the design lifetime is:

$$\tilde{F}_0^{radial\_linT} = \lambda \Delta T_0^{design} \left[\frac{1}{2R} + \frac{4}{3} \left(\frac{\rho c}{\lambda \pi \Delta t_0^{design}} \right)^{1/2} \right] \tag{14}$$

Equations (8) and (12) can be used to estimate temperature as a function of distance from the reservoir at all times. In particular, a compliance distance ($R^{compliance}$) can be estimated as the distance at which temperature decline is a specified value at a specified time. For example, an operating company may want to limit thermal interference between EGS reservoirs developed at different times or operating at different temperatures, or a regulatory agency may have the same requirement for reservoirs with different operators, by specifying a limit of a 10 ºC decline outside of the permitted region during the 30 years of operation. In that case, the size of the permitted area is the area occupied by the sphere of radius $R + R^{compliance}$.

Similarly, when computing heat extraction efficiency (the fraction of total usable heat that has been extracted over the design lifetime), it is necessary to estimate the volume of rock from which heat has been removed, so some extraction radius $R + R^{extraction}$ is used for the efficiency estimate:

$$heat\ extraction\ efficiency = \frac{total\ heat\ removed}{\frac{4}{3}\rho c \Delta t_0^{design} \pi (R + R^{extraction})^3} \tag{15}$$

The heat removed from the reservoir proper ($r < R$) over the design lifetime is:

$$Q^{reservoir} = \dot{Q}^{reservoir} \Delta t_0^{design} = \frac{4}{3} q \Delta t_0^{design} \pi R^3 \tag{16}$$

where Q (units of J) is the heat, and the heat flow rate is $\dot{Q}$ (units of J s^{-1}) is designated with the dot over the heat. A lower bound estimate of heat removed from outside the reservoir ($r > R$) over the design lifetime is given by the linear-decline estimate:

$$Q^{outside\_lower} = \dot{Q}^{outside\_lower} \Delta t_0^{design} = 4 \tilde{F}_0^{radial\_linT} \Delta t_0^{design} \pi R^2 \tag{17}$$

And the upper estimate is:

$$Q^{outside\_upper} = \dot{Q}^{outside\_upper} \Delta t_0^{design} = 4 F_0^{radial} \Delta t_0^{design} \pi R^2 \tag{18}$$

The average heat delivery rate for the reservoir ($\dot{Q}$, inside plus outside) is bounded in the range given by the inequality:

$$\left| \frac{4\pi R^3}{3} \frac{2F_0}{b} + 4\pi R^2 \tilde{F}_0^{radial\_linT} \right| < |\dot{Q}| < \left| \frac{4\pi R^3}{3} \frac{2F_0}{b} + 4\pi R^2 F_0^{radial} \right| \tag{19}$$

allowing an estimate for heat (and therefore power) production for a powerplant of known well and fracture spacing. The absolute value is used because the sign convention implicitly assumes heat extracted is negative heat, converting equation (19) to a statement about the magnitude of heat delivered from the reservoir to a power plant. Equations (15)-(19) give a bounded estimator for heat extraction efficiency in the range:

$$\left| \frac{\frac{4\pi R^3}{3} \frac{2F_0}{b} \Delta t_0^{design} + 4\pi R^2 \tilde{F}_0^{radial\_linT} \Delta t_0^{design}}{\frac{4\pi (R + R^{extraction})^3}{3} \rho c \Delta T_0^{design}} \right| < heat\ extraction\ efficiency < \left| \frac{\frac{4\pi R^3}{3} \frac{2F_0}{b} \Delta t_0^{design} + 4\pi R^2 F_0^{radial} \Delta t_0^{design}}{\frac{4\pi (R + R^{extraction})^3}{3} \rho c \Delta T_0^{design}} \right| \tag{20}$$

As expected, the extraction efficiency depends on the assumed extent of the reservoir, with computed efficiency declining when a larger distance away from the reservoir is included in the efficiency calculation. Recall that R is a function of well spacing, and $\frac{2F_0}{b}$ (the reservoir heat supply per volume, or more simply, the heat supply density) is only a function of fracture spacing and the design lifetime of the power plant.

2.3 Regional maps of EGS potential

To estimate the upper limit of EGS resource potential, it is necessary to estimate how closely spaced operating geothermal reservoirs can be without thermal interference. The closest possible spacing is the highest efficiency geometry. Assuming power plants are similarly sized, the Kepler conjecture states that the maximum volume of closely packed spheres is ~74% of the total volume (proven by Hales (2005)). Using the upper and lower bounds of heat supply from outside the reservoir (equations (14) and (11), respectively), this implies that an upper limit power production density for EGS powerplants is bounded by:

$$0.74 * \left| \frac{\left[\frac{4\pi R^3}{3} \frac{2F_0}{b} + 4\pi R^2 \tilde{F}_0^{radial\_linT} \right]}{\frac{4\pi (R + R^{compliance})^3}{3}} \right| < |\tilde{q}| < 0.74 * \left| \frac{\left[\frac{4\pi R^3}{3} \frac{2F_0}{b} + 4\pi R^2 F_0^{radial} \right]}{\frac{4\pi (R + R^{compliance})^3}{3}} \right| \tag{21}$$

where $\tilde{q}$ has units of (W m^{-3}) and the first term in the square brackets is energy produced from within the reservoir, the second term is energy flowing into the reservoir from outside, and the numerator is the participating area sphere. Using equation (20), recognizing that the left-hand term is the lower estimate of heat extraction efficiency (ϵ^{lower}) and the right-hand term is the upper estimate (ϵ^{upper}), equation (21) can be rewritten:

$$0.74 * \epsilon^{lower} \left| \frac{\rho c \Delta T_0^{design}}{\Delta t_0^{design}} \right| < |\tilde{q}| < 0.74 * \epsilon^{upper} \left| \frac{\rho c \Delta T_0^{design}}{\Delta t_0^{design}} \right| \quad (22)$$

where the term in absolute values is the steady energy production rate if heat extraction efficiency was 100% (units of W/m^3). This corresponds to the total available heat (above the minimum temperature).

Either equation (21) or (22) works equally well for $\tilde{q}$, and therefore three-dimensional maps of EGS heat production density can be constructed from a three-dimensional temperature map (e.g., Burns and others, 2024). To estimate heat production density for each location, ΔT is computed as the difference between the mapped temperature and the minimum temperature for electricity production, and temperature is used to correct thermal conductivity for computations using the relation of Williams and DeAngelo (2011). Multiplying by a success factor ($0 \leq \beta \leq 1$) would give heat production value for assessments ($\tilde{q}_H^{assessment}$), and in general, β will vary as a function of location (i.e., geology at depth). To get EGS electricity production density, a conversion efficiency from heat to electricity can be added using a spatially variable coefficient $0 \leq \varepsilon \leq 1$, which in general is a function of temperature and the engineered components converting heat to electricity. To make two-dimensional maps (units of W m^{-2}), heat production density is integrated vertically. Herein, only one map is created. This map integrates $\left| \frac{\rho c \Delta T_0^{design}}{\Delta t_0^{design}} \right|$, allowing the use of equation (22) to evaluate the impact of fracture spacing, the distance between wells, and recovery and conversion efficiencies on total estimated EGS resource potential for the Great Basin.

For EGS assessment computations herein, it is assumed that $R^{compliance} = R^{extraction}$, and $R^{extraction}$ is selected to be the distance away from the reservoir where 0.5% of the design temperature decline (ΔT_0^{design}) occurs at the end of operations (e.g., for a 200 ºC decline, the distance away from the reservoir where there is a 1 ºC drop after 30 years of operation). In practice, operations may require a safety factor for distance, which would increase $R^{compliance}$, with the result that the estimate of EGS resource potential for the region will be smaller.

RESULTS AND DISCUSSION

First, we compare with previous numerical modeling results to assure that simplifications used for the new analytical solution provide reasonable estimates. We then evaluate the influence of well and fracture spacing, and construct EGS potential maps.

3.1 Single Reservoir Estimates of Heat Production, Electricity Generation, and Recovery Efficiency

Equations (4)-(20) can be used to make estimates for single-reservoir heat and electricity production. To ensure that estimates are reasonable, results herein are compared with simulation results summarized in Figure 6 of Sanyal and Butler (2005). Sanyal and Butler consider a range of fracture spacings and well geometries, but Figure 6 is the only figure summarizing a simulation where fluid flow is through a zone of sufficient permeability (100 md horizontal) to allow a constant flow rate test with constant injection temperature (82 ºC) and temperature approaching 82 ºC at approximately 30 years (similar to conditions for models herein). All other simulations had variable or otherwise limited flow rate. Additional conditions include a five-spot well geometry within a fracture zone of dimensions 914 m by 914 m by 304.8 m with fracture spacing of 30.5 m. The initial uniform temperature of the reservoir is 210 ºC. Sanyal and Butler assume thermal to electric conversion efficiency is 10%. Volumetric heat capacity (the product ρc) is set to 2,000 kJ m^{-3} ºC^{-1}, so for this comparison, the specific heat capacity is set to be 740.74 J kg^{-1} ºC^{-1} to match Sanyal and Butler's heat capacity. The thermal conductivity of the rock is not listed in the manuscript, so is assumed to be 2.7 W m^{-1} ºC^{-1} (c.f., Williams and DeAngelo, 2011). Assuming the design temperature drop is 210 ºC minus 82 ºC, and a spherical reservoir of the same volume as the Sanyal and Butler volume for Figure 6 (corresponds to a sphere of radius 393.3 m), equation (19) yields a predicted average gross electricity production of about 8 MWe.

Unlike the equations derived herein to estimate sustainable, nearly steady heat and electricity production, Sanyal and Butler consider a steady injection rate with a constant injection temperature (high initial heat production that declines more rapidly for early times). As a result, Sanyal and Butler show gross electricity production that varies smoothly (concave up) from ~43 to ~11 MWe over 30 years. Because Sanyal and Butler simulate injecting a constant temperature fluid, the boundary condition temperature near the injection well is below all curves in Figure 2, indicating that heat extraction is higher near the injection well. Temperature near the extraction well declines at a rate similar to one of the curves below the dashed line in Figure 2. As a result of the more aggressive heat extraction (lower injection temperature) and three-dimensional heat sweeping, the Sanyal and Butler estimate is higher than estimates made using simplified equations developed herein.

Assuming that the radius used for computation of heat extraction efficiency is the distance from the fractured reservoir where temperature decline is ~1 ºC (corresponding to 116 m away from the fractured reservoir; Figure 3), efficiency is predicted (equation (20)) to be in the range 53.4-55.4%. Sanyal and Butler estimate heat "recovery" of 60.7% for their "stimulated volume", so that our estimated heat extraction efficiency reasonably agrees with Sanyal and Butler's heat recovery, given their higher average heat extraction rate. The slightly lower efficiency estimates from methods derived herein are conservative values likely resulting from the assumption of uniform heat extraction rather than the real-life more efficient heat extraction nearer the injector well where temperature gradients are highest.

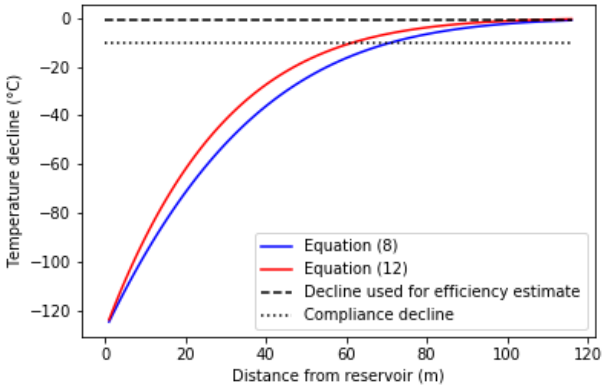

Figure 3: Estimates of temperature (after 30 years of operation) as a function of distance from the fractured reservoir (conditions are from Sanyal and Butler, 2005, their Figure 6). For estimation of $R^{extraction}$, a value of 1 °C decline is used to calculate heat recovery efficiency. A regulatory agency might set a compliance point beyond which a decline of a certain magnitude is not allowed (an example shows a 10 °C decline, corresponding to a distance in the range of 60-70 m from the fractured reservoir). Temperatures will continue to evolve after 30 years as a function of continued reservoir operations.

3.2 The Effects of Fracture Spacing, Reservoir Size, and Temperature on Single Reservoir Performance

In this section, we evaluate the influence of fracture spacing, reservoir size, and temperature on the estimated steady heat delivery rate (megawatts-thermal; MWth) from a single power plant and the corresponding heat extraction efficiency. The left-hand panel of Figure 4 shows the advantage of connecting wells over a larger distance, which yields a reservoir with substantially higher energy production for all effective fracture spacings. However, the right-hand panel shows that heat delivered per volume of rock is much less variable. In other words, if a lease is provided for a specific area / volume, heat extraction might be accomplished with multiple shorter well connections, yielding only a slightly smaller recovery efficiency over the life of the project.

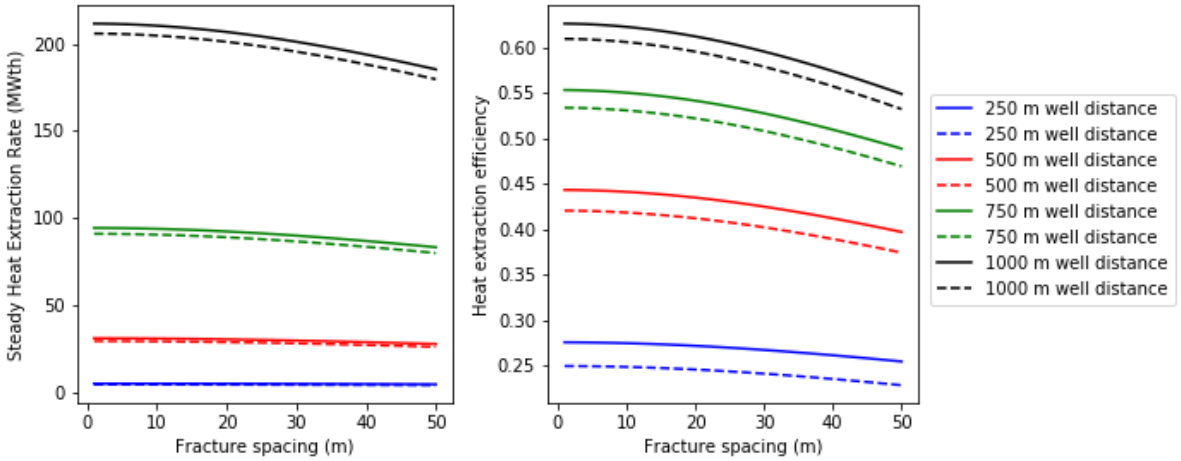

Figure 4: For a design temperature decline of 150 °C, upper (solid lines) and lower (dashed lines) estimates of heat extraction rate (left) and heat extraction efficiency (right). For these estimates, bulk thermal conductivity is held constant at 2.7 W m^{-1} $°C^{-1}$.

Figure 5 shows heat extraction efficiency as a function of design temperature drop (ΔT) assuming bulk thermal conductivity is constant. Because $R^{extraction}$ is set as a fraction (0.5%) of the design temperature drop, and the rate of transmission of the boundary condition is controlled by a constant diffusivity (if thermal conductivity is constant), then heat extraction efficiency is not a function of ΔT. In other words, once heat extraction efficiency is computed for a given well distance and fracture spacing, the efficiency will not change as ΔT changes, so the efficiency estimates from Figure 4 apply to all ΔT.

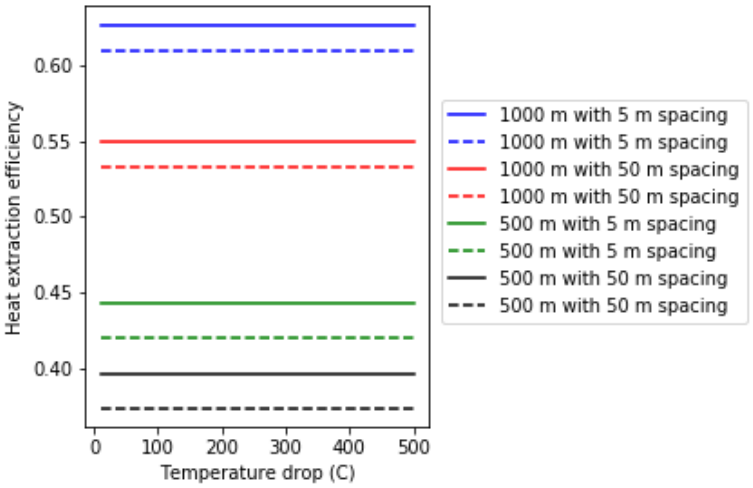

Figure 5: Varying design temperature decline is a function of thermal diffusivity, so does not affect heat extraction efficiency for a given well and fracture spacing, provided bulk thermal conductivity is constant. For these estimates, bulk thermal conductivity is held constant at 2.7 W m^{-1} ºC^{-1}.

To evaluate the influence of temperature-dependent bulk thermal conductivity on heat extraction efficiency, ΔT was fixed at 100 ºC, and the relation of Williams and DeAngelo (2011) was used:

$$\lambda(\mathrm{T}) = \frac{\lambda_0}{a + bT} \tag{23}$$

where λ_0 is thermal conductivity at 0 °C (set herein to be 2.7 W m^{-1} ºC^{-1}) with $a = 1.0$ and $b = \left(0.0024 - \frac{0.0052}{\lambda_0}\right)$.

Figure 6 has an odd saw-tooth character that is the result of how the algorithm estimates $R^{extraction}$ (estimated to the nearest whole meter), but the overall shape is instructive. As temperature increases, thermal conductivity decreases, and for a fixed $R^{extraction}$, heat recovery efficiency decreases slowly. This lower recovery efficiency also decreases the necessary $R^{extraction}$ distance, and at the point where the nearest whole-meter distance decreases, then both the lower and upper estimates from equation (20) increase. The net effect from low to high temperature is an increase in heat extraction efficiency because the total volume of affected rock is smaller. In other words, EGS reservoirs can be more closely spaced at higher temperatures. In practice, this apparent benefit does not exist if the ultimate plan is to substantially lower temperatures. The net effect of varying temperature across a wide range of values expected in the upper 7 km of the Earth's crust is that, for a given well and fracture spacing, heat recovery efficiency might vary by 1-2% as a function of temperature (Figure 6).

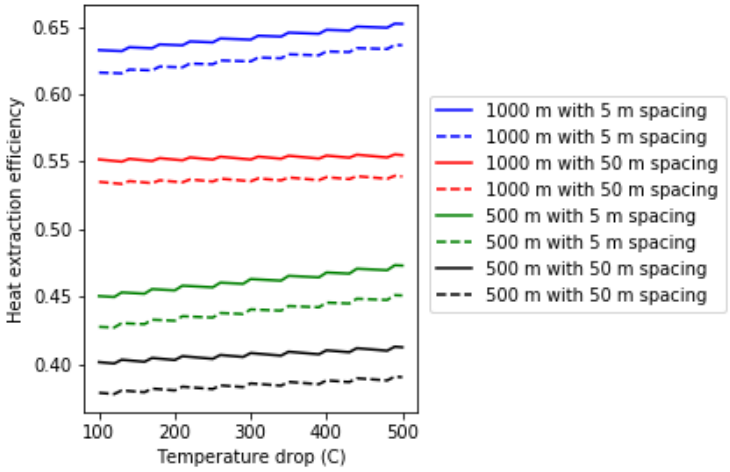

Figure 6: For a design temperature decline of 100 C, allowing bulk thermal conductivity to vary as a function of temperature results in a minor increase in heat extraction efficiency as temperature increases.

3.3 EGS Estimates for the Great Basin

The net result from Figures 4-6 is that estimates made for heat recovery efficiency using Equation (20) (e.g., right-hand Figure 4) can be used to estimate EGS resource potential using Equation (22). Estimates made from equation (22) can vary spatially as a function of geology, so use of this relation implicitly assumes that there are three-dimensional maps of geology for which stimulation (e.g., fracturing) conditions are known. In particular, it assumes that the achievable effective fracture spacing and distance over which wells are connected by these fractures is known.

To make a two-dimensional map of EGS potential, equation (22) is integrated over depths where temperature is greater than T_{min} (the temperature below which generation of electricity is not possible; assumed herein (for demonstration) to be the Sanyal and Butler [2005] value of 82 ºC for computations herein):

$$\int_{z(T>T_{min})} \varepsilon * \beta * 0.74 * \epsilon^{lower} * \left| \frac{\rho c \Delta T_0^{design}}{\Delta t_0^{design}} \right| dz < \tilde{Q} < \int_{z(T>T_{min})} \varepsilon * \beta * 0.74 * \epsilon^{upper} * \left| \frac{\rho c \Delta T_0^{design}}{\Delta t_0^{design}} \right| dz \quad (24)$$

where $\tilde{Q}$ is the EGS heat generation potential at each map location (W m^{-2}). All efficiencies are within the integral, which allows for the likelihood that each parameter changes as a function of depth. For the Great Basin, these three-dimensional properties are not currently known, so for the following estimates and comparisons, it is assumed that $\varepsilon, \beta, \epsilon^{lower}$, and ϵ^{upper} are uniform, allowing a simplified evaluation of the effects of different fractures and well spacing:

$$\varepsilon * \beta * 0.74 * \epsilon^{lower} \int_{z(T>T_{min})} \left| \frac{\rho c \Delta T_0^{design}}{\Delta t_0^{design}} \right| dz < \tilde{Q} < \varepsilon * \beta * 0.74 * \epsilon^{upper} \int_{z(T>T_{min})} \left| \frac{\rho c \Delta T_0^{design}}{\Delta t_0^{design}} \right| dz \quad (25)$$

Using the temperature estimates of Burns and others (2024), a map of the value of the integrand for depths above 7 km is shown in Figure 7. This integral is 100% of the electric-grade heat above 7 km divided by the 30-yr design lifetime, giving the amount of heat that could be delivered if perfectly extracted. Actual heat production, accounting for inefficiencies and conversions, is estimated by multiplying by the coefficients in equations (24) and (25). Equation (24) allows for the general case where these factors depend spatially on the reservoir geology and stimulation success.

Maximum 30-yr heat production ranges from 140 to 1,568 W m^{-2} (average of 741 W m^{-2}). Uniformly applying the Keppler closest spacing factor of 0.74, and assuming that on-average heat extraction efficiency could be engineered to 0.5 (c.f., right-hand Figure 4), 30-yr EGS heat production capacity ranges from 52 to 580 W m^{-2} (average of 274 W m^{-2}) if all geologic layers could be developed. If 25% of the geologic units are favorable for EGS, and a heterogeneity factor of 0.1 is applied (c.f., Williams, 2010), and these layers are randomly distributed (e.g., some shallow and some deep), then $\beta = 0.025$, and 30-yr EGS heat production capacity is lowered to 1.3—14.5 W m^{-2} (average of 6.9 W m^{-2}). Integrating over the Great Basin, the total EGS heat resource would be 4,340 GWth for 30 years (down from 174 TWth if $\beta = 1.0$). If technology only allows development of the resource at depths above 5 km (essentially $\beta = 0.0$ deeper than 5 km), then the electric-grade resource is 34% of the resource from depths shallower than 7 km, and the total EGS electric resource would be 1,490 GWth for 30 years.

Recall that Williams and others (2008) estimated 520 GWe for the western United States from resources >150 ºC shallower than 6 km. Crudely assuming thermal to electric conversion efficiencies in the range 0.1-0.25 gives reasonable agreement between Williams and estimates made with the methods developed herein. As technology improves, increasing the number of viable geologic layers (depth and lithology) that can be successfully stimulated, and improving extraction technologies to account for heterogeneity (i.e., a net increase in β from 0.025 towards the theoretical maximum of 1.0), the results herein demonstrate that the electric generation potential could exceed the estimates of Williams and others.

As technology improves, the heterogeneity factor (assumed to be 0.1 [10%] above) increases, and the number of viable geologic units increases, the estimated heat extraction rates (here >10x greater than the background heat flow) will increase to greater than 100x greater than the natural background conductive heat flow, indicating full-scale geothermal energy development with improved heat extraction rates would not be renewable. These estimates indicate that heat would be mined at an unsustainable rate and, after 30 years of operation, the resource would be nearly depleted unless technology advances to allow the development of other geologic layers (i.e., β increases over time). Another possibility is that reservoir life could be extended substantially by storing surplus electric-grade heat within the reservoir during periods of excess (e.g., Zhang and others, 2024).

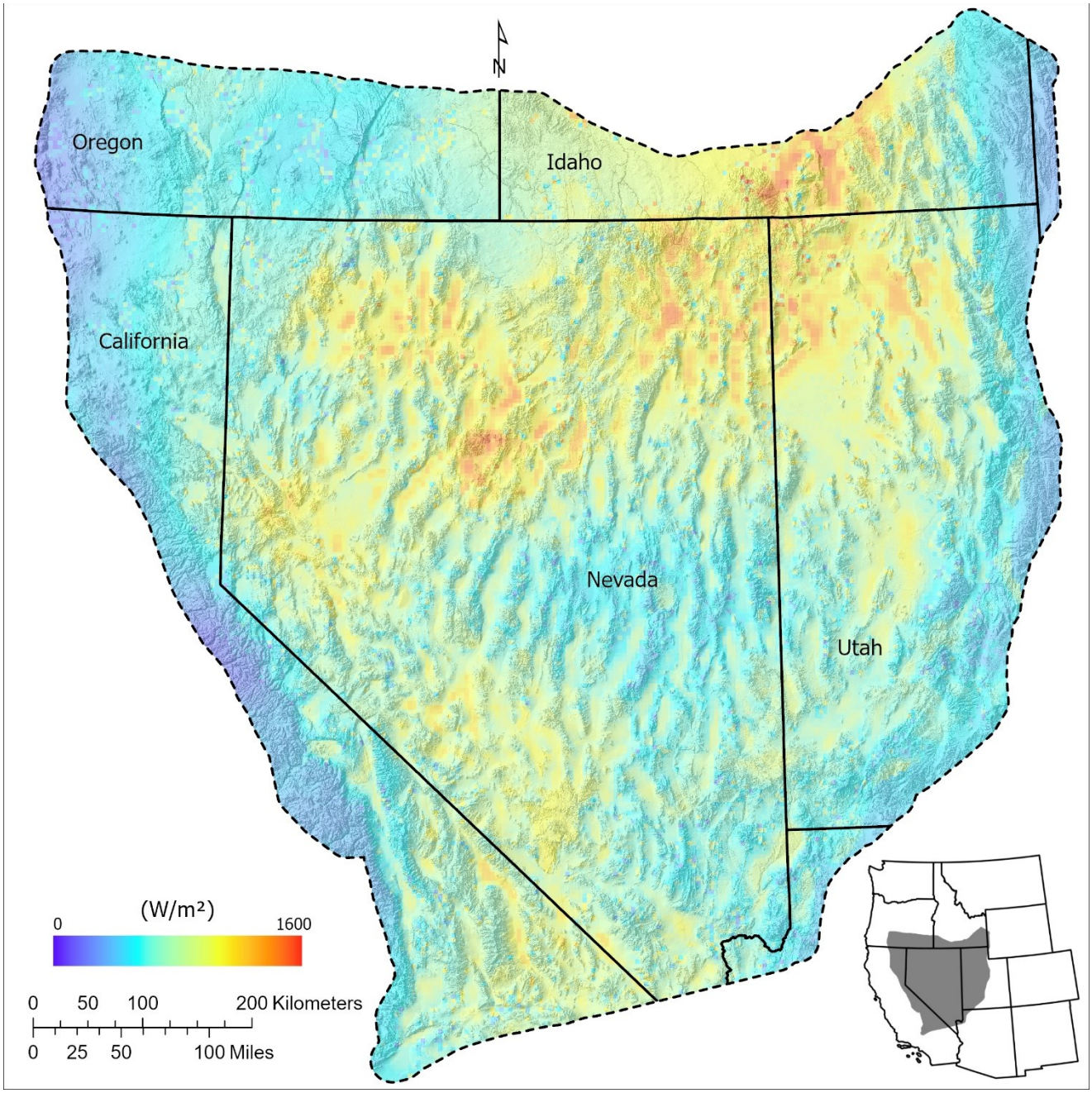

Figure 7: Map of maximum 30-yr heat production from electric-grade temperature shallower than 7 km depth (integrand from equation (25)). Maximum heat production is the theoretical maximum, assuming 100% heat extraction efficiency. Hillshade is derived from USGS National Atlas (National Atlas of the United States, 2012).

SUMMARY AND LIMITATIONS

EGS assessment strategies have been improved to account for the effects of fracture spacing and length (i.e., well distance) on heat extraction. Computations assume that heat production will occur at an approximately steady rate over the life of the power plant and that at the end of design life (e.g., 30 years), production temperatures will be at the minimum for producing electricity (i.e., the reservoir is maximally utilized). It is implicitly assumed that fracture spacing, fracture permeability, and pumping rates can be engineered to extract heat as required. For a range of well distances (250-1,000 m), heat extraction efficiency ranges from 25-62%, and estimates are given to support regulatory agencies that set compliance distances. By far the biggest uncertainty in estimating the EGS resource for the Great Basin is estimating which geologic units, at what depths, can actually be stimulated sufficiently to economically produce geothermal energy (e.g., 30-year estimates of heat production range from ~1.5 to ~174 TWth).

Although the analytic approximations developed herein compare favorably and conservatively with some more complex three-dimensional models (see section 3.1), Horne and Temeng (1995) demonstrate complexities in fluid flow and heat extraction that may need

to be evaluated further when considering individual EGS powerplants. In other words, though the analyses herein are instructive and likely conservative, care should be taken when using estimates for other purposes, and there is no substitute for site-scale data collection and analyses.

The following improvements in understanding would allow systematic refinement of estimates of EGS resource potential for the Great Basin:

1) A three-dimensional geologic model of lithologic units of the Great Basin, USA, to the depth above which EGS technologies are proven to be viable (determined by currently viable drilling and stimulation practices).
2) A three-dimensional model of stress/strain conditions (which determine how a geologic unit can be stimulated).
3) Quantitative understanding of fracture length and spacing as a function of 1) and 2) above, based on experimental evidence from drilling and stimulation experiments.
4) As the number of operating EGS powerplants increases, statistics of electric power generation over time will help to constrain models.
5) Better-constrained relationships defining heat-to-electric conversion efficiency as a function of temperature would also improve electric production estimates. Generally, conversion efficiency declines with temperature, but not in a linear way. Herein, a uniform lower temperature of 82 ºC (taken from Sanyal and Butler, 2005) is adopted in a naïve way. Conversion of available heat will be a function of technology (e.g., steam flash, binary, etc.), and minimum pre-development temperature is not considered herein (e.g., electricity would not be developed unless parasitic loads of the powerplant are substantially exceeded).

ACKNOWLEDGEMENTS

This study was funded by the U.S. Geological Survey Energy Resources Program and the U.S. Department of Energy - Geothermal Technologies Office under award DE-EE0009254 to the University of Nevada, Reno for the INnovative Geothermal Exploration through Novel Investigations Of Undiscovered Systems (INGENIOUS). Any use of trade, firm, or product names is for descriptive purposes only and does not imply endorsement by the U.S. Government.

REFERENCES

Abramowitz, M., & Stegun, I.A., Handbook of Mathematical Functions, With Formulas, Graphs, and Mathematical Tables. (1965). Dover Publications, Inc.

Aljubran, M.J., Horne, R.N., 2024, Power supply characterization of baseload and flexible enhanced geothermal systems. Sci Rep 14, 17619 (2024). https://doi.org/10.1038/s41598-024-68580-8.

Augustine, C., Fisher, S., Ho, J., Warren, I., and Witter, E., Enhanced geothermal shot analysis for the geothermal technologies office, Technical report, (2023), National Renewable Energy Laboratory (NREL), Golden, CO (United States).

Burns, E.R., DeAngelo, J., and Williams, C.F., Updated three-dimensional temperature maps for the Great Basin, USA, Proceedings 49th Stanford Geothermal Workshop, Stanford, California, February 12-14, 2024, SGP-TR-227, (2024a).

Burns, E.R., DeAngelo, J., and Williams, C.F., Three-dimensional temperature model of the Great Basin, USA: U.S. Geological Survey data release, https://doi.org/10.5066/P149FR54, (2024b).

Carslaw, H. S., and Jaeger, J. C. Conduction Heat in Solids. Oxford University Press, U.S.A.; 2nd edition, (1986), ISBN-10: 0198533683

Chabora, E., Zemach, E., Spielman, P., Drakos, P, Hickman, S., Lutz, S., Boyle, K., Falconer, A., Robertson-Tait, A., Davatzes, N.C., Rose, P., Majer, E., and Jarpe, S., Hydraulic Stimulation of Well 27-15, Desert Peak Geothermal Field, Nevada, USA, Proceedings 37th Stanford Geothermal Workshop, Stanford, California, January 30-February 1 (2012).

Crank, J., The Mathematics of Diffusion. Oxford University Press. 2nd edition, (1975), ISBN-10: 9780198534112

DeAngelo, J., Burns, E.R., Gentry, E., Batir, J.F., Lindsey, C.R., Mordensky, S.P., Heat flow maps and supporting data for the Great Basin, USA: U.S. Geological Survey, (2022), https://doi.org/10.5066/P9BZPVUC.

DeAngelo, J., Burns, E.R., Gentry, E., Batir, J.F., Lindsey, C.R., Mordensky, S.P., New Maps of Conductive Heat Flow in the Great Basin, USA: Separating Conductive and Convective Influences, Proceedings 48th Stanford Geothermal Workshop, Stanford, California, February 6-8, (2023).

Elsworth, D., A comparative evaluation of the parallel flow and spherical reservoir models of HDR geothermal systems: J. Volcanol. Geotherm. Res., 44: 283-293, (1990).

Hales, T.C., A proof of the Kepler conjecture: Annals of mathematics, 162, (2005), 1065-1185.

Horne, R.N., and Temeng, K.O., Relative Productivities and Pressure Transient Modeling of Horizontal Wells with Multiple Fractures: SPE Middle East Oil Show, Bahrain, 11-14 March 1995, SPE 29891, (1995).

McClure, M.W., and Horne, R.N., An investigation of stimulation mechanisms in Enhanced Geothermal Systems: International Journal of Rock Mechanics & Mining Sciences, 72, 242-260, (2014), http://dx.doi.org/10.1016/j.ijrmms.2014.07.011.

National Atlas of the United States, 100-Meter Resolution Elevation of the Conterminous United States. National Atlas of the United States, (2012). Available at: http://purl.stanford.edu/zz186ss2071.

Oldham, K., Myland, J., & Spanier, J.. AN ATLAS OF FUNCTIONS, (2009). Springer. 2nd edition.

Sanyal, S.K., and Butler, S.J., An Analysis of Power Generation Prospects from Enhanced Geothermal Systems: GRC Transactions, Vol. 29, (2005).

Tester, J. (Panel chair) and others, The Future of Geothermal Energy: Impact of Enhanced Geothermal Systems (EGS) on the United States in the 21st Century, Idaho National Lab Report INL/EXT-06-11746, Massachusetts Institute of Technology, Cambridge, Massachusetts, 374p, (2006).

Williams, C. F., 2010, Challenges in the Assessment and Classification of Enhanced/Engineered Geothermal System Resources: GRC Transactions, Vol. 34.

Williams, C. F., and DeAngelo, J., Evaluation of Approaches and Associated Uncertainties in the Estimation of Temperatures in the Upper Crust of the Western United States: GRC Transactions, Vol. 35, (2011).

Williams, C. F., Reed, M.J., Mariner, R.H., DeAngelo, J., and Galanis, S.P., Assessment of Moderate-and High-Temperature Geothermal Resources of the United States: U.S. Geological Survey Fact Sheet 2008-3082, U.S. Geological Survey Fact Sheet 2008-3082, pp. 1–4, (2008), http://pubs.usgs.gov/fs/2008/3082/.

Zhang, J.Y., Burns, E.R., and Zhan, H.B., The Advantages of Electric-grade Heat Storage in Long Closed-loop Wells: Geothermal Rising Conference Transactions, (2024).

APPENDIX A (DERIVATION OF NEW SOLUTION)

To model heat conduction from a sphere into the infinite domain surrounding the sphere, the governing equation can be written as:

$$\frac{\partial T}{\partial t} = D\left(\frac{\partial^2 T}{\partial r^2} + \frac{2}{r}\frac{\partial T}{\partial r}\right) \tag{A.1}$$

where T is the temperature [Θ], D is the thermal diffusion coefficient [L^2T^{-1}] and is derived from $D= k/\rho c$ (c, ρ, and k are specific heat capacity [$L^2T^{-2}\Theta^{-1}$], density [ML^{-3}], and thermal conductivity [$MLT^{-3}\Theta^{-1}$] of the material, respectively), T is time [T] and r is the location at any point of concern in the space[L]. In this question, the initial temperature in the research domain is 0, the temperature at the surface of the sphere is increased with time, and at a very long distance from the sphere, the temperature is zero. Therefore, the related initial condition and boundary conditions are as follows:

$$T(r, t = 0) = 0 \tag{A.2}$$

$$T(r = \infty, t) = 0 \tag{A.3}$$

$$T(r = a, t) = kt \tag{A.4}$$

where a is the radius of the sphere [L] and k is a temperature increased rate at the surface [ΘT^{-1}].

This equation can be converted to a pseudo one-dimensional equation by applying $u=Tr$, the same approach has been used in much previous research (Crank, 1975; Carslaw and Jaeger, 1986). Then the Eqs. (A.1) – (A.4) will become:

$$\frac{\partial \mathrm{u}}{\partial t} = D\left(\frac{\partial^2 \mathrm{u}}{\partial r^2}\right) \tag{A.5}$$

$$u(r, t = 0) = 0 \tag{A.6}$$

$$u(r = \infty, t) = 0 \tag{A.7}$$

$$u(r = a, t) = akt \tag{A.8}$$

Applying Laplace transform to Eqs. (A.5) – (A.8) with respect to t, one will have the following equations in Laplace space:

$$p\bar{u} = D\frac{d^2\bar{u}}{dr^2} \tag{A.9}$$

$$\bar{u}(r = \infty) = 0 \tag{A.10}$$

$$\bar{u}(r = a) = \frac{ak}{p^2} \tag{A.11}$$

where p is the Laplace transform operator and $\bar{u}$ is the Laplace transform of u in Laplace domain. And the general solution of Eq. (A.9) can be written as:

$$\bar{u} = C_1 e^{\frac{\sqrt{p}}{\sqrt{D}}r} + C_2 e^{-\frac{\sqrt{p}}{\sqrt{D}}r} \tag{A.12}$$

where C_1 and C_2 are unknown constant coefficient and can be calculated with boundary conditions.

By applying Eq. (A.10) to Eq. (A.12), one has:

$$C_1 = 0 \tag{A.13}$$

By applying Eqs. (A.11) & (A.13) to Eq. (A.12), one can obtain:

$$C_2 = \frac{ak}{p^2} e^{\frac{\sqrt{p}}{\sqrt{D}}a} \tag{A.14}$$

Therefore, the final solution with the boundary condition in Laplace space can be written as:

$$\bar{u} = \frac{ak}{p^2} e^{\frac{\sqrt{p}}{\sqrt{D}}a} e^{-\frac{\sqrt{p}}{\sqrt{D}}r} = \frac{ak}{p^2} e^{-\frac{\sqrt{p}}{\sqrt{D}}(r-a)} \tag{A.15}$$

To solve u in time domain, we first define $f(p) = \frac{ak}{p}$ and $g(p) = \frac{1}{p} e^{-\frac{\sqrt{p}}{\sqrt{D}}(r-a)}$, where $f(p)$ and $g(p)$ are the Laplace transform of $F(t)$ and $G(t)$ respectively. Then Eq. (15) can be written as $\bar{u} = f(p)g(p)$. Using the Convolution Theorem (Eq. 29.2.8 in Abramowitz and Stegun (1965)), u can be expressed as:

$$u = \int_0^t F(t-\tau)G(\tau)\, d\tau \tag{A.16}$$

and $F(t)$ and $G(t)$ can be calculated by (Eq. 29.3.2 and Eq. 29.3.83 in Abramowitz and Stegun (1965)):

$$F(t) = ak \tag{A.17}$$

$$G(t) = \operatorname{erfc}\left(\frac{r-a}{2\sqrt{Dt}}\right) \tag{A.18}$$

Because we are interested in the region from sphere surface to the infinite domain, we use the case $r>a$ for $G(t)$. Applying Eqs. (A.17) and (A.18) to Eq. (A.16), the result of u is:

$$u = \int_0^t ak \operatorname{erfc}\left(\frac{r-a}{2\sqrt{D\tau}}\right) d\tau = ak \int_0^t \operatorname{erfc}\left(\frac{r-a}{2\sqrt{D\tau}}\right) d\tau \tag{A.19}$$

Recalling that the relation of T and u is $u = Tr$. Therefore, the final solution of T is:

$$T(r,t) = \frac{u}{r} = \frac{ak}{r} \int_0^t \operatorname{erfc}\left(\frac{r-a}{2\sqrt{D\tau}}\right) d\tau \tag{A.20}$$

By defining $A = \frac{ak}{r}$ and $B = \frac{r-a}{2\sqrt{D}}$, and using integration by parts, the solution can be simplified to the following:

$$T(r,t) = A\left\{\left[\tau * \operatorname{erfc}\left(\frac{\mathrm{B}}{\sqrt{\tau}}\right)\right]\Big|_0^t - \frac{B}{\sqrt{\pi}} \int_0^t \frac{e^{-B^2/\tau}}{\sqrt{\tau}} d\tau\right\} \tag{A.21}$$

where the differentiation of erfc function is given in Oldham and others (p409, 2009).

Substituting $\frac{B^2}{\tau}$ by ω, one can obtain:

$$T(r,t) = A\left\{\left[\tau * \operatorname{erfc}\left(\frac{\mathrm{B}}{\sqrt{\tau}}\right)\right]\Big|_0^t - \frac{B^2}{\sqrt{\pi}} \int_{\frac{B^2}{t}}^{\infty} \frac{e^{-\omega}}{\omega^{1.5}} d\omega\right\} \tag{A.22}$$

where the right part is called upper incomplete gamma function (Abramowitz & Stegun, 1965) and can be written as

$$T(r,t) = A\left\{\left[\operatorname{erfc}\left(\frac{r-a}{2\sqrt{Dt}}\right)\mathrm{t}\right] - \frac{B^2}{\sqrt{\pi}} \Gamma\left(-0.5, \frac{B^2}{t}\right)\right\} \tag{A.23}$$

with $A = \frac{ak}{r}$ and $B = \frac{r-a}{2\sqrt{D}}$.

And one important property (Abramowitz & Stegun, 1965) of the upper incomplete gamma function is

$$\Gamma(a+1,x) = a\Gamma(a,x) + x^a e^{-x}$$

or

$$\Gamma(a,x) = \frac{\Gamma(a+1,x) - x^a e^{-x}}{a}$$

This property can be used to calculate the upper incomplete gamma function with a negative a value.

Calculate the flux that passes through the sphere surface:

Differentiate formulation of T (r, t) in Eq. (A.20) with respect to r and applying the chain rule, the flux at any point of concern can be written as:

$$\frac{\partial}{\partial r}T(r,t) = -\frac{ak}{r^2}\int_0^t \operatorname{erfc}\left(\frac{r-a}{2\sqrt{D\tau}}\right)d\tau + \frac{ak}{r}\frac{\partial\left[\int_0^t \operatorname{erfc}\left(\frac{r-a}{2\sqrt{D\tau}}\right)d\tau\right]}{\partial r} \quad (A.24)$$

By exchanging the rank of integral and differentiation, Eq. (A.24) can also be written as:

$$\frac{\partial}{\partial r}T(r,t) = -\frac{ak}{r^2}\int_0^t \operatorname{erfc}\left(\frac{r-a}{2\sqrt{D\tau}}\right)d\tau + \frac{ak}{r}\int_0^t \frac{\partial\left[\operatorname{erfc}\left(\frac{r-a}{2\sqrt{D\tau}}\right)\right]}{\partial r}d\tau \quad (A.25)$$

After differentiation, Eq. (A.24) becomes:

$$\frac{\partial}{\partial r}T(r,t) = -\frac{ak}{r^2}\int_0^t \operatorname{erfc}\left(\frac{r-a}{2\sqrt{Dc}}\right)d\tau + \frac{ak}{r}\int_0^t \left(-\frac{1}{\sqrt{D\pi\tau}}e^{-\frac{(r-a)^2}{4D\tau}}\right)d\tau \quad (A.26)$$

At the boundary, the flux that passes through the sphere surface is:

$$flux = -K\frac{\partial}{\partial r}T(r=a,t) = K\left(\frac{kt}{a} + \frac{2k\sqrt{t}}{\sqrt{D\pi}}\right) \quad (A.27)$$

where K is the thermal conductivity of the spherical domain [LT^{-1}].